Optimization of building-integrated photovoltaic thermal air system combined with thermal storage

Yetao Xiang* **and Guohui Gan**
Faculty of Engineering, Energy and Sustainability Division, University of Nottingham, Nottingham, UK

Abstract

Photovoltaic (PV) combined with phase change material (PV/PCM) system is a hybrid solar system that uses a PCM to reduce the PV temperature and to store energy for other applications. This study aims to increase the integrated PV efficiency of buildings by incorporating PCM while utilizing the stored heat in PCM for controlling indoor conditions. Experiments have been carried out on a prototype PV/PCM air system using monocrystalline PV modules. Transient simulations of the system performance have also been performed using a commercial computational fluid dynamics package based on the finite volume method. The results from simulation were validated by comparing it with experimental results. The results indicate that PCM is effective in limiting temperature rise in PV device and the heat from PCM can enhance night ventilation and decrease the building energy consumption to achieve indoor thermal comfort for certain periods of time.

Keywords: photovoltaic; phase change material; hybrid solar; BIPV

*Corresponding author.
laxyx6@nottingham.ac.uk

Received 13 November 2014; revised 13 March 2015; accepted 15 March 2015

1 INTRODUCTION

There are factors that can affect the efficiency of a photovoltaic (PV) panel, among which the operating temperature of the PV cell could be a very important one. High operating temperatures lead to a drop in the electrical conversion efficiency at a rate of ~0.5%/°C for crystalline PV cells. In summer, the cell temperature can reach 70°C which reduces the conversion efficiency by 22.5% drop from the standard test conditions [1]. In recent years, great attentions have been paid to control the PV cell temperature. Researchers have tried out various techniques including active cooling and passive heat removal [2, 3]. Active cases usually use a pump or fan to circulate water or air to cool the PV panel. Passive methods involve the use of a duct at one or both sides of PV for natural ventilation, or high heat capacity material such as PCM at the back of PV for direct absorbing heat.

In a building-integrated PV (BIPV) system, passive heat removal usually relies on buoyant flow of air through an opening or an air channel duct at either front or back of the PV panel [4]. Yun *et al.* [5] presented an investigation on a naturally ventilated wall-integrated PV system with an opening behind the PV. The results indicated a monthly maximum temperature reduction of 5°C due to natural ventilation leading to an annual increase of 2.5% in an electrical output of the PV.

In residential buildings, solar energy is usually lowest when the thermal requirement is most, which makes the thermal energy storage systems very important in solar thermal application. Energy demands in buildings vary on daily, weekly and seasonal bases. Thermal energy storage systems can help with these demands. The use of thermal energy storage for thermal application such as space and water heating, cooling and air conditioning also has recently received much attention. Phase change material (PCM) has been proved a great thermal control material in the building environment field [6–8]. Researches have shown that incorporating PCM with certain designed melting temperature similar to the PV characterizing temperature for the thermal regulation of BIPV under cyclic time-dependent solar energy input is a promising approach to temperature control. At the same time, the energy stored in the PCM can be released to provide building heating and enhance natural ventilation at night.

Huang *et al.* [9] presented an experimental investigation on which the PCM was contained in an aluminum box with its front surface coated with a solar absorption material to represent PV cell attached to its front. They performed a study on the temperature distributions on the front surface and inside PCM with and without fins at different insolation. They also developed 2D and 3D finite volume heat transfer simulation models to investigate PCM performance for BIPV thermal regulation [10, 11].

International Journal of Low-Carbon Technologies 2015, 10, 146–156

doi:10.1093/ijlct/ctv010 Advance Access Publication 20 April 2015

Hasan *et al.* [2] attached a PV module to a rectangular aluminum box containing PCM which was irradiated at 415 W/m^2. The result showed a 10°C temperature reductions for 6 h compared with a PV attached to the box without PCM.

Most of investigations on PV/PCM were focused on energy store and release of PCM only, and less attention was paid to combining the convection factor into the model or experiment. In reality, the heat transfer at the back side of the PV/PCM system varies with the ambient condition, and it will be helpful if this heat transfer can be enhanced. This study aims to increase the PV efficiency by incorporating PCM while utilizing the stored heat from PCM for conditioning indoor air.

2 MATERIALS AND METHODS

The literature review indicates that modeling of phase change and natural convection processes presents a significant challenge, due to complexity of the involved physical phenomena [12]. On the other hand, natural air flow is always difficult to predict due to its uncontrollable behavior. In this study, computational fluid dynamics (CFD) was used to simulate the two processes together.

There are two main thermal characteristics during the phase change, enthalpy temperature relationship and temperature hysteresis. The ANSYS Fluent code was used to solve the governing equations. The default model of phase change in the software is an enthalpy-porosity model which treats the solidified region as a porous medium. The porosity in each cell is set equal to the liquid fraction in that cell and appropriate momentum sink terms are added to the momentum equations to account for the pressure drop caused by the presence of a solid material [13]. In fully solidified regions, the porosity is equal to zero, which extinguishes the velocities in these regions. The mushy zone is a region in which the liquid fraction lies between 0 and 1. Its properties are determined using a lever rule based on the difference between the melting and freezing temperatures. The lever rule calculates the density, viscosity and heat capacity of the mushy zone based on a proportionally weighted average of the liquid and solid properties. Susman *et al.* [14] employed the enthalpy-porosity method to simulate PCM sails and found that the method produced reasonable temperature prediction in global space temperature terms. Assis *et al.* [15] carried out a numerical and an experimental investigation of the melting process of RT27 with a PCM in a spherical geometry filled with 98.5% solid PCM as an initial condition of the simulation. They concluded that CFD is an effective way to study the PCM.

Boussinesq approximation was used for natural air flow because the variations in temperature and density are small. At the same time, variations in volume expansion due to temperature gradients will also be small. The purpose of this study is to optimize the design of BIPV/PCM system, so some assumptions have been made to simplify the simulation process and reduce computation time: (a) thermophysical properties of the material are constant for liquid and solid. (b) Thermal expansion and motion of the PCM due to phase change are neglected because PCM made from hydrated salt has very small thermal expansion factor and because the magnitude of estimated velocity in the fully melted PCM is only about 0.0001 m/s. (c) Contact resistance between the PCM and container is neglected.

2.1 Initial settings of simulated CFD model

A two-dimensional PV/PCM air model is presented in Figure 1 and boundary conditions are labeled. The model consists of a layer of thick aluminum box filled with PCM on the left side and air duct on the right side.

For a transient state simulation, the time step and grid size independence studies have been carried out in preliminary calculations. In particular, four different time steps were tested: 0.1, 0.2, 0.5 and 1 s. As can be seen from Figure 2, the results obtained for temperature and velocity vary at beginning, but then become independent of the time step after a certain time, 50 s for temperature and 600 s for velocity. Figure 3 shows the difference in velocity at certain position in the model between time step 0.1 and 1 s at time 1000 s. It has a maximum difference of ~12.5% and average of 5% errors.

So, in order to reduce the calculation time, 0.1 s time step was used at beginning for all the simulations, and then after 600 s, the time step was increased to 1 s.

Mesh size was also investigated based on temperature and velocity. As for natural ventilation, the recommended mesh (edge) size should be smaller than 1 mm. A fine mesh size of 1 mm was taken as the benchmark. Three mesh sizes are studied and the details are shown in the Table 1. Figure 4 shows the temperature of PV surface for the three cases. It can be found that the difference is quite small between case 1 with fine mesh, and about 2% difference between case 2 and fine mesh. Table 2 shows all the observed points position used in this study.

The coupled wall boundary condition is specified at the interface between PCM and air duct to allow heat transfer. The second-order upwind scheme was used for solving the pressure, momentum and energy equations and the transient formulation. Fixed heat fluxes

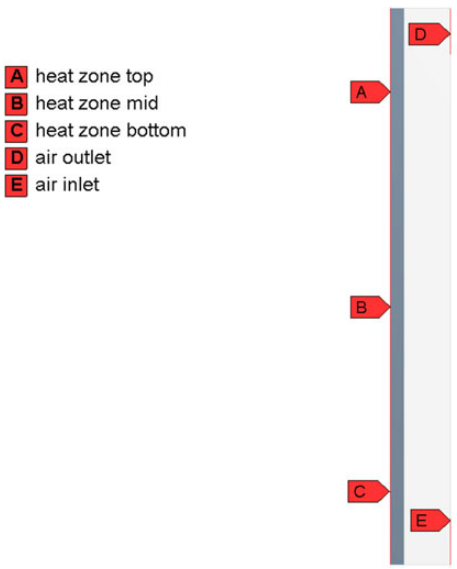

Figure 1. *Boundary conditions for two-dimensional CFD model.*

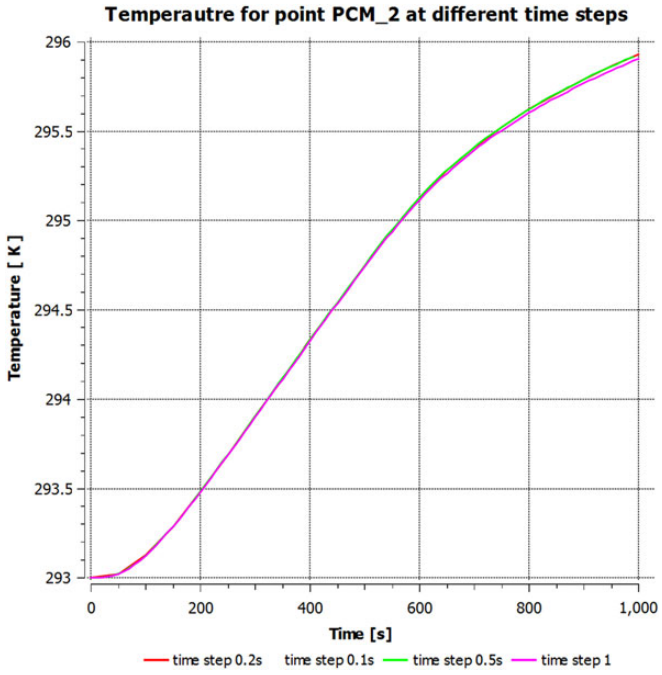

Figure 2. *Temperature at point 2 four different time steps.*

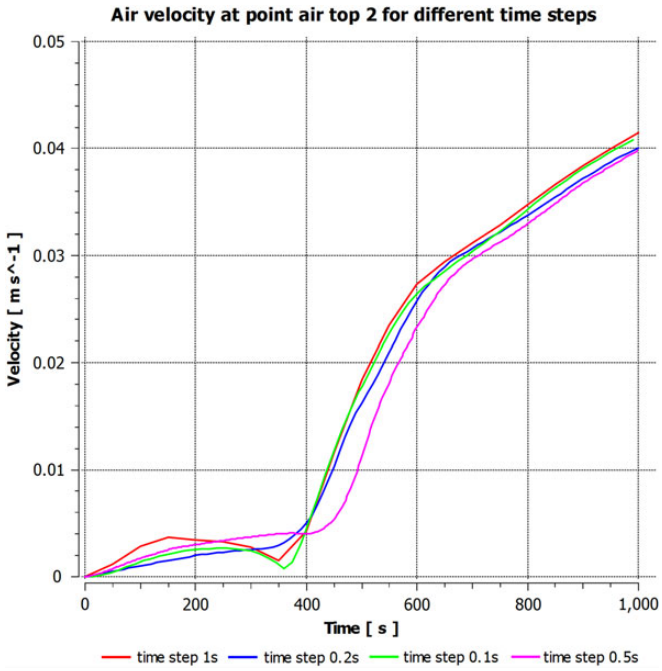

Figure 3. *Air velocity at air top point 2.*

were applied at the PV face (position ABC in Figure 1), so the heat transfers from PV to PCM through conduction and then transfer to air through convection. The fixed heat fluxes were calculated based on the solar intensity, heat removal factor from convection and radiation at front side. From measurements of artificial lights in experiment, three heat fluxes 400, 500, and 400 W were applied to three heat zones on the PV for validation purpose. Position E in Figure 1 is air inlet for duct, in natural ventilation case; it is specified as a

Table 1. *Mesh size.*

	Edge size	Total cell number
Mesh 1	1 mm	1 56 000
Mesh 2	1.25 mm	99 840
Mesh 3	2.5 mm	24 960

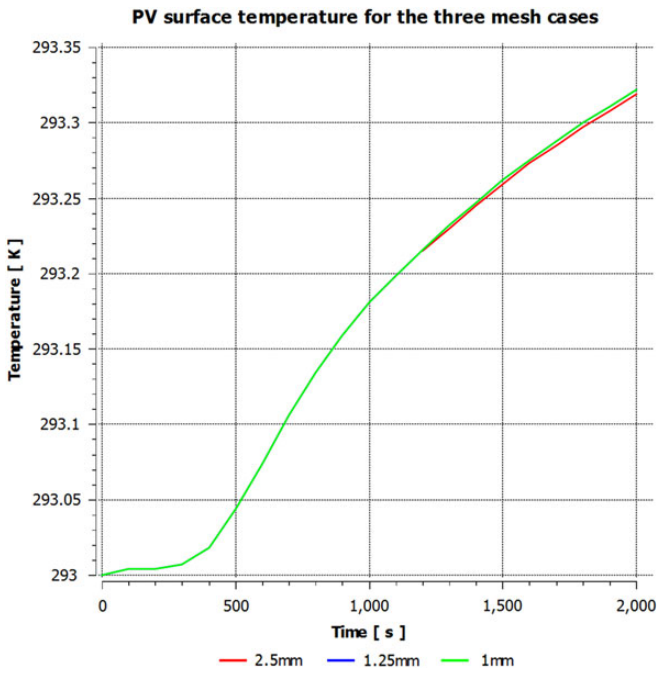

Figure 4. *PV temperature for the three mesh cases.*

Table 2. *Observed points.*

Point	*X*	*Y*	Point	*X*	*Y*
PCM_1	0	0.6	PCM_8	0.03	0.1
PCM_2	0.1	0.6	Air bot 1	0.04	0.1
PCM_3	0.02	0.6	Air bot 2	0.09	0.1
PCM_4	0.3	0.6	Air mid 1	0.04	0.6
PCM_5	0	1.1	Air mid 2	0.09	0.6
PCM_6	0.03	1.1	Air top 1	0.04	1.15
PCM_7	0	0.1	Air top 2	0.09	1.15

pressure inlet. Position D is the pressure outlet in most cases. All other walls are well insulated and no heat transfer takes place. The initial conditions are specified based on the measured data. Solidifying process was simulated after 10 h by turning off the lights, and lowering the ambient temperature to 15°C.

2.2 Experiment set up

A schematic view of the physical model is presented in Figure 5. The experimental tests were carried out on a prototype PV/T air system using two commercial monocrystalline PV modules rated at 100 W each at standard test conditions and about 0.65 m^2 each as absorber plate. The specification of PV panel was listed in Table 3.

To construct the test unit and ensure high conductivity, an aluminum box (1200 mm × 1100 mm) was made and filled with

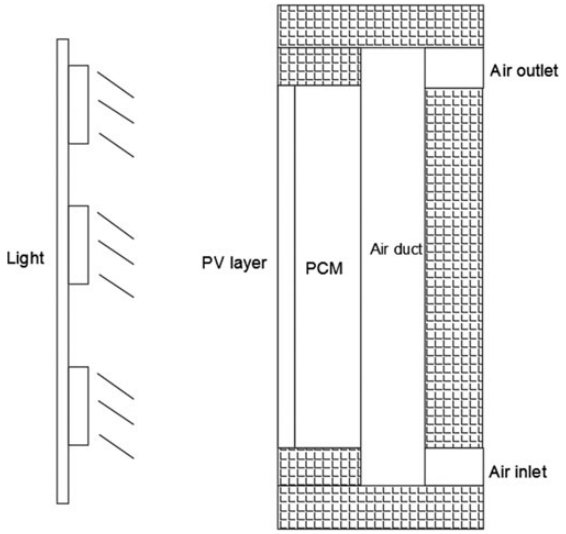

Figure 5. *Physical model of whole test unit.*

Table 3. *Specification of PV panel.*

Peak power (P_{max})	100 W
Cell type	Monocrystalline
Maximum power voltage (V_{mp})	19.3 V
Maximum power current (I_{mp})	5.18 A
Open circuit voltage (V_{oc})	22.9 V
Short circuit current (I_{sc})	5.56 A
Maximum system voltage	750 V
Temp. coeff. of I_{sc} (TK I_{sc}) temp.	0.06 $\pm$ 0.01
Coeff. of V_{oc} (TK Voc) Temp.	$-$(78 $\pm$ 10)
Coeff. of P_{max} (TK P_{max})	$-$(0.5 $\pm$ 0.05)
Normal operating cell temperature	48 $\pm$ 2°C
Power tolerance	$-$3% to +3%
Dimension (mm)	1200 × 540 × 30 mm
Weight (kg)	8 kg
Solar cells	36(4 × 9)

PCM (PLUSICE S25). To accommodate possible thermal expansion, 2% volume was left for air in the container. An aluminum box with adjustable depth (20 mm, 30 mm, 50 mm) was made to optimize the volume of PCM required. A rectangular air duct box was designed, with adjustable channel depth from 0 to 250 mm and constructed to accommodate the PV module on the top and bottom using Celotex Insulation board of thickness 100 mm, which also serves as back and side insulations (Figure 6). The PV panel were mounted in the front of the aluminium box, with thermal paste between them to enhance the conduction. Simulated insolation was produced by nine 500 W artificial lights (Figure 7).

The PCM used in this study, PLUSICE S25, is supplied by Phase Change Material Products Ltd. It is made from hydrates salt and freezes and melts at temperature of 25°C. The specification of this PCM is shown in Table 4.

Twenty-three T type thermocouples with an accuracy of $\pm$0.1 K were distributed inside the test cell and on the walls. Twelve thermocouples were located at three identical depths within the PCM to measure spatial temperature variations. Six thermocouples were positioned equidistantly on the front and back

Figure 6. *Photograph of insulation position and inlet and out let of air duct.*

Figure 7. *Photograph of artificial lights and their position.*

surfaces to measure surface temperatures and three thermocouples were placed along the air duct to measure air temperature.

The air velocity was measured by a hot wire anemometer, with accuracy of $\pm$0.02 m/s. The simulated solar energy from artificial light was measured by a solar power meter. Before the test start, a uniformity test for the radiation intensity was performed. The results show that the radiation varied up to 20% from midpoint to side. At midpoint, the intensity reached 500 W/m^2 while at the edge it only had 400 W/m^2. So, in order to getter better performance in simulation work, the PV panel was divided into three heat zones, with different solar intensities. A plate ammeter shunt (10 A, 75 mV) and two 100 W resistor were connected and used to investigate the electrical efficiency of

Table 4. *Thermo physical properties of PCM.*

PCM type	Phase change temperature	Density	Latent heat capacity	Volumetric heat capacity	Specific heat	Thermal conductivity	Volumetric expansion 1/kg %
S25	25°C	1530 kg/m^3	180 kJ/Kg	275 MJ/m^3	2.2 kJ/kg K	0.54 W/m K	2

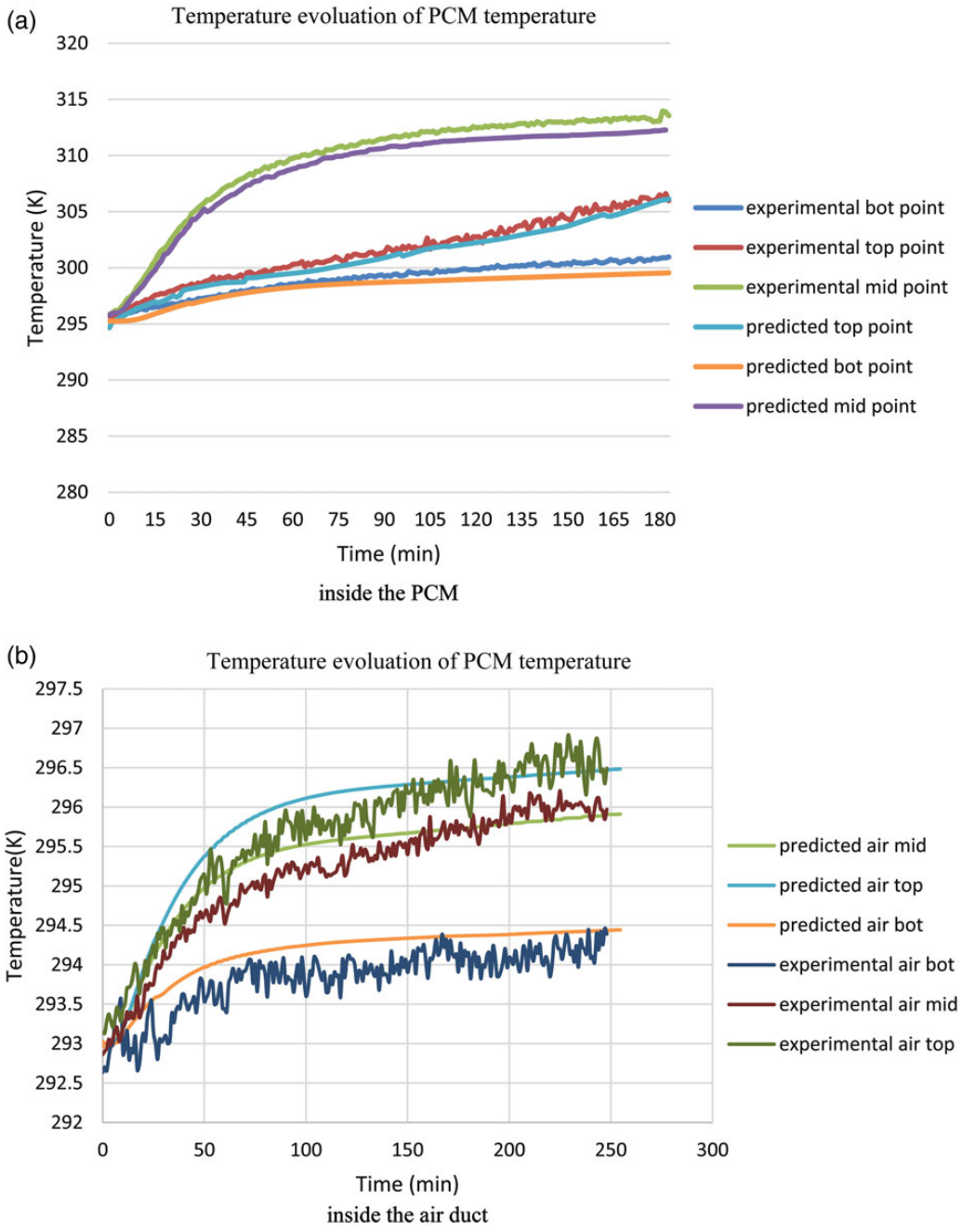

Figure 8. *Predicted and experimental transient temperatures at three points. (a) Inside the PCM. (b) Inside the air duct.*

the PV panel. All temperature data and electrical data of PV were recorded at an interval of 1 min by a DT800 data logger. Before each experiment was started, it was ensured that all temperatures in the cell were at the steady state, for the valid initialization of the CFD models. This would take about 10 h.

2.3 Validation

The validation is based on the dynamic evolution of temperature and air velocity at various points in the test cell, compared with the experimental data. A list of observed points is presented in Table 2. Figure 8a shows the experimental and simulated

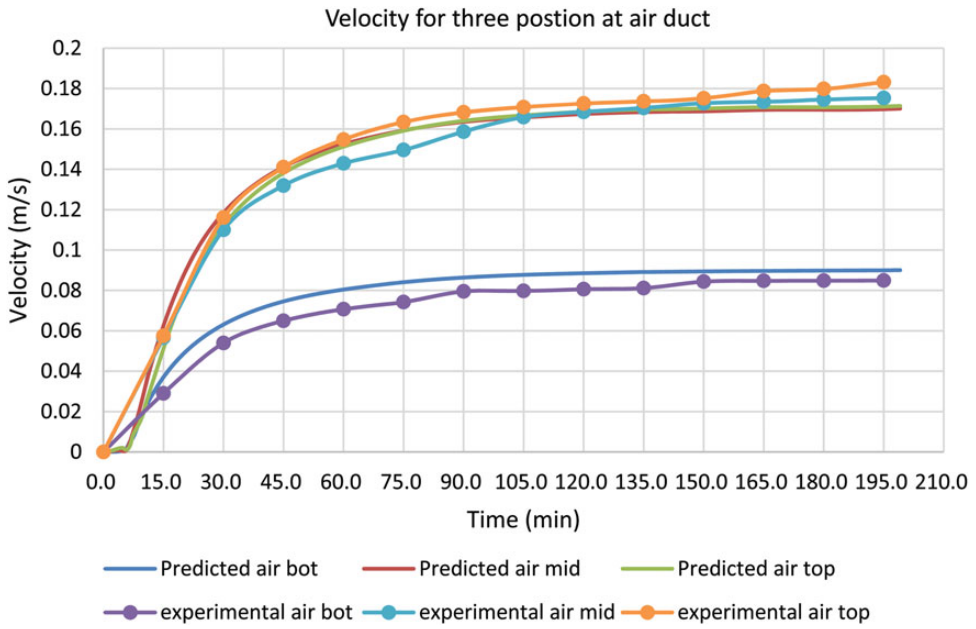

Figure 9. *Predicted and experimental transient velocity of three points in the air duct.*

Table 5. *List of simulated cases.*

Case	PCM container thickness (mm)	Air duct thickness (mm)
1	30	100
2	50	100
3	30	50
4	40	100

temperatures of three thermocouples in the PCM unit. The temperature curves of experiment and simulation are very close to each other, with a maximum difference of about 8%. However, the predicted temperature is slightly lower than the experimental one.

Figure 8b shows the predicted transient temperature of three points in the air duct. The agreement between experiment and numerical simulation is reasonable. However, the difference between experimental and predicted results is larger than the temperature in PCM. For lower temperatures obtained, the difference on average is $\sim$1.0°C and, for the higher temperatures, the difference differs $\sim$3.5°C between the two results. The possible sources of error for the simulation include neglecting the conduction resistance of the container box, the natural convection inside the PCM and radiation heat transfer and the uncertainty in the thermocouples ($\pm$0.2 K) and other instrumentation.

Air velocity was recorded at an interval of 15 min for three positions for validation purpose. Figure 9 shows predicted and experimental transient velocity of three points in the air duct. All curves from simulation follow the result trend from experiment. However, the air velocity has $\sim$10% larger relative error than temperature validation. This may be due to the low magnitude of velocity in the natural ventilation and the limitation of hot wire anemometer with relatively large uncertainty. Laser Doppler velocimetry (LDV) is a suggestion for more accurate measurement.

In conclusion, the CFD model is reasonable and valid. The numerical model was used to predict natural ventilation and heat transfer performance of the whole unit and results are presented below.

3 RESULTS AND DISCUSSION

3.1 Effect of PCM and air duct size

The numerical model presented before was used to carry out a parametric study. The same initial conditions were used for all the simulations and four different cases were listed in Table 5.

Figure 10 shows the mean air velocity magnitude at the air outlet. Case 1 has the largest air velocity compared with other cases; the velocity would rapidly increase at $\sim$280 min. The sharp increase also happened to Case 3, which might be due to melting of the PCM layer in contact with the back side of the container which greatly increased the temperature, and then heat transfer near the air outlet greatly increased. Cases 2 to 4 have the same trend at first, but the velocity for Case 3 increased quicker and also increased suddenly at 280 min. No sudden increase was observed for Cases 2 and 4 for 340 min because they both have thicker layer of PCM and require more time for the interface of melting to reach the back. The results show that the thickness of both PCM and air duct affects the natural ventilation. Large velocity is preferred if ventilation is required, which usually results in large heat transfer rate to indoor environment. Although thicker layer of PCM can provide more heat capacity for maintaining temperature, it has lower ability for natural

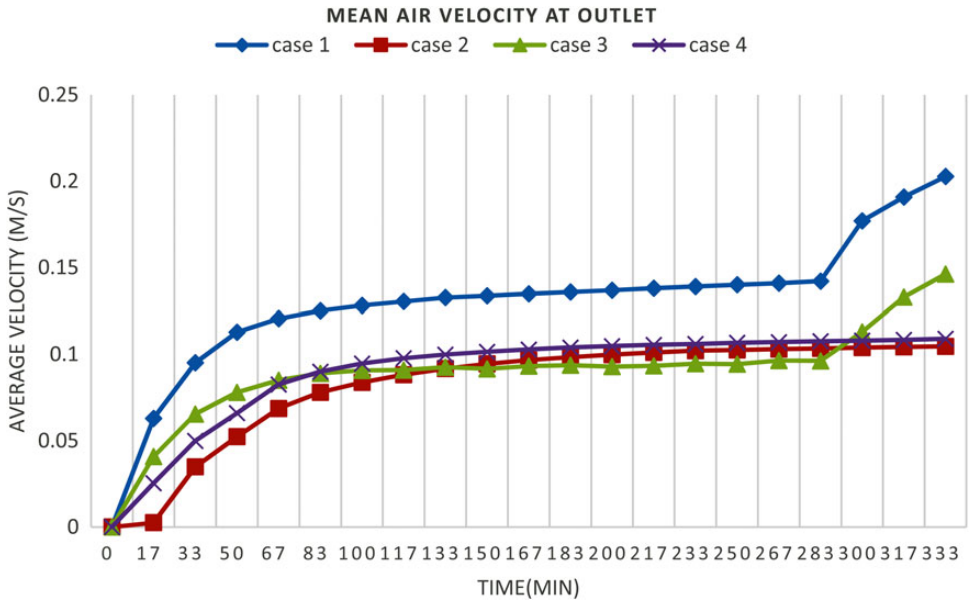

Figure 10. *Mean air velocity at air outlet.*

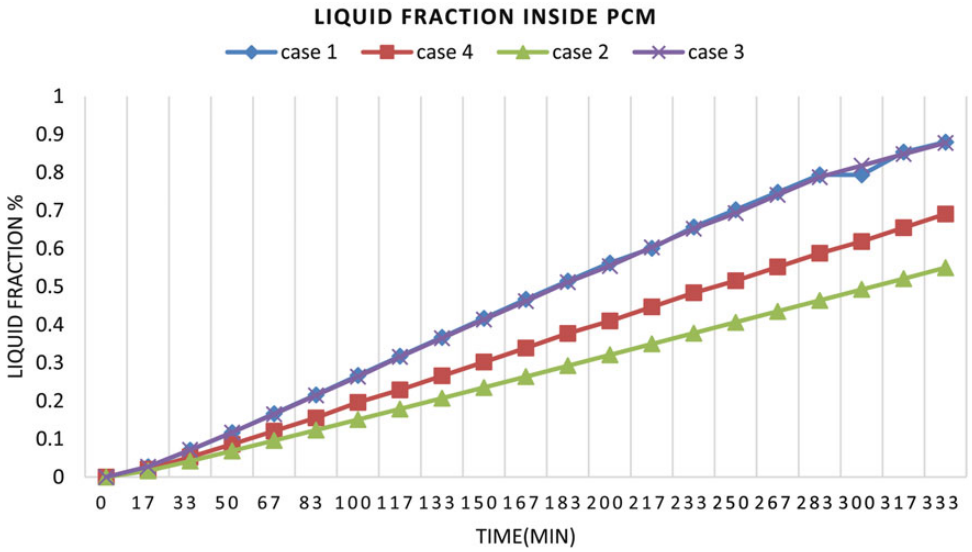

Figure 11. *Liquid fraction in the PCM container.*

ventilation and presents a problem of too long time of melting and solidifying.

One important advantage of simulation was to provide data which is difficult to obtain in an experiment, for example, liquid fraction versus time in a sealed container. Figure 11 shows the liquid fraction in the PCM container for different cases. PCM for Cases 1 and 3 melted fastest because of thinner PCM layer and higher heat transfer rate from natural ventilation and that in Case 2 melted slowest because of the thickest layer. Cases 1 and 3 have different sizes of air duct but result in same trend of liquid fraction along time, which suggests that natural convection may have limited effect on removing heat because melting results from solar heat absorption rather than natural convection which in fact has the opposite effect—cooling.

The temperature of PV panel is very important because it controls the electrical performance. Figure 12 shows the average temperature of the PV panel. All the cases have the same trend before 300 min, which maintains the PV temperature below its operating temperature, 318 K. After then, PCM for Case 3 almost fully melted as can be found from Figure 11, and the temperature went up quickly. However, the temperature for Case 1 which has the

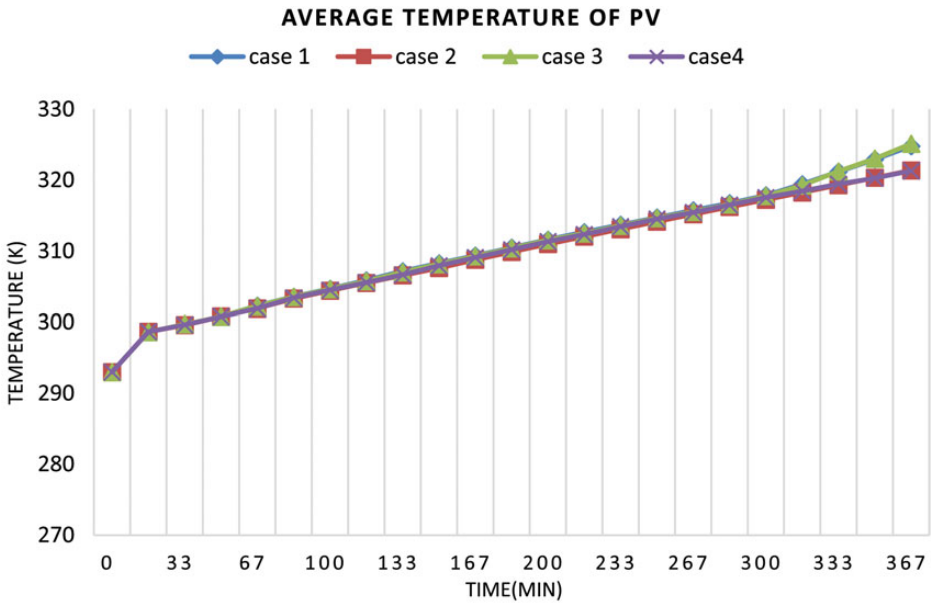

Figure 12. *Average temperature of PV panel.*

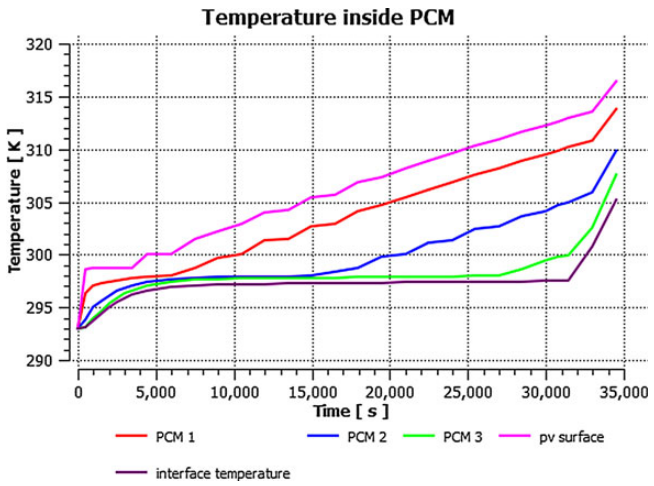

Figure 13. *Temperature at different points.*

same thickness of PCM which had nearly fully melted still keeps the same rate of increase. This is due to the large natural convection for Case 1, which has a better of heat removing factor than Case 3. Therefore, the air duct size is also important in designing a PV/PCM air system.

3.2 Simulation for real environment

The CFD model was also applied to simulate a real condition. Solar intensity was set to 600 W/m^2 to simulate the average solar intensity on a vertical wall at a typical sunny day in summer time in Nottingham. To illustrate the system operation, Figure 13 shows various temperatures and the PCM phase over a 10-h period for the system.

Figure 13 shows the variations with time of the PCM's temperature at different observed points. It is obvious that melting starts at point 1 and spreads to other points melt later depending on their position. The rear side of PCM has fully melted at ~8.75 h when the interface temperature increases sharply. It can maintain the PV temperature below its normal operating cell temperature of 321 K for ~9.7 h which is sufficient to prevent overheating of PV for a typical UK sunny day with such a high insolation.

Figure 14 shows velocity and temperature distributions in air duct at 3000 and 10 000 s. The maximum velocity at 3000 s is about 0.194 m/s near the bottom back of aluminum box and the average is 0.13 m/s at outlet. At 10 000 s, maximum velocity increased to 0.328 m/s.

Simulation was also performed for the solidifying process with natural ventilation for night cooling. The air temperature was fixed at 15°C.

Figure 15 shows the temperature distribution in PCM in solidifying process. Temperature of PV surface dropped rapidly due to high heat convection at front side which is exposed to outside, and the temperature at back of PCM dropped slowly due to solidifying process and low convection heat transfer in the indoor condition. It takes almost 16.67 h for full solidification which would occur in only if the following day is cloudy or raining. So, either forced convection or fins in the PCM are required to increase the heat removal.

The PV/PCM wall of the experiment had ~0.035 m^3 of volume of PCM and total mass of about 54 kg. So, the maximum energy saving is ~9.6 MJ, equal to 2.67 kW h. In this case, if the PCM works 9 h at maximum performance, one PCM cycle can store 24 kW h energy that can reduce certain amount of the energy demand from HVAC system per day.

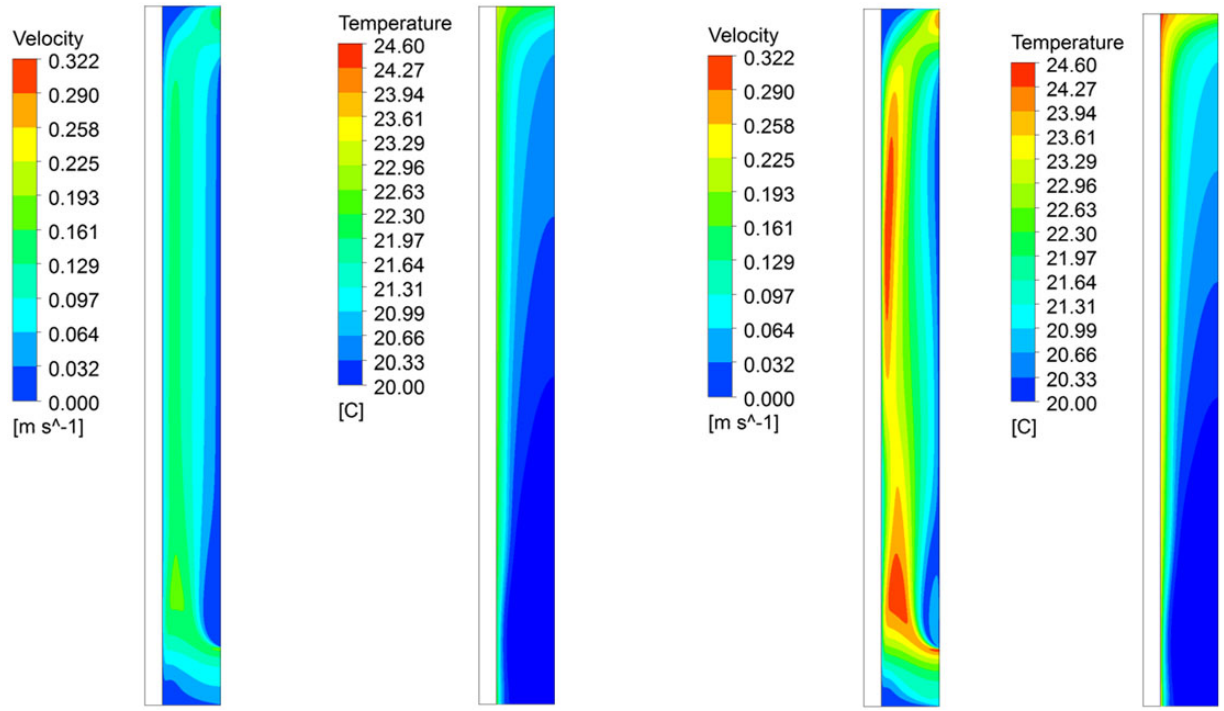

Figure 14. *Velocity and temperature distributions contours in air duct at time 3000 s (left) and 10 000 s (right).*

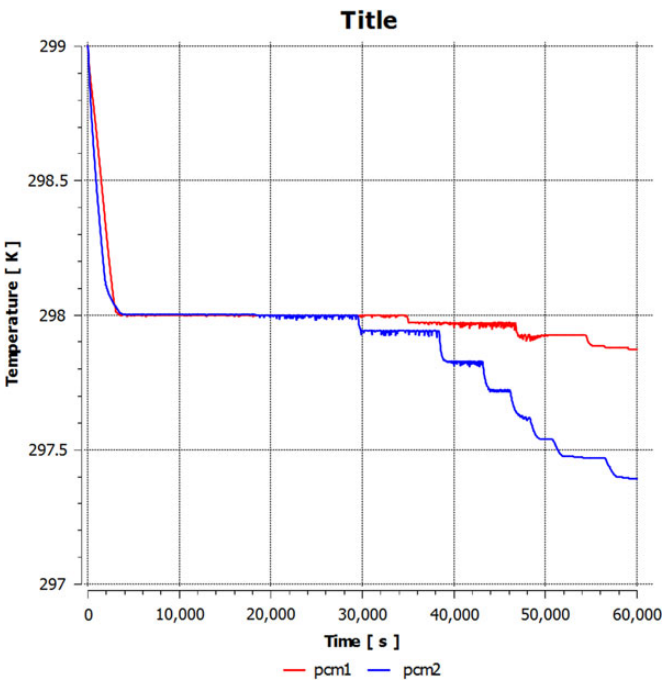

Figure 15. *Temperature for PV surface and back in PCM in solidifying process.*

3.3 Effect of fins

Figure 16 shows the schematic diagram of PV/PCM system with horizontal fins inside PCM.

A simulation was carried out with horizontal fins inserted inside the PCM to improve heat conduction inside the PCM.

Figure 16. *Schematic diagram of PV/PCM system with fins inside PCM.*

Figure 17 shows the temperature at three observed points in PCM. Compared with Figure 13, the total melting time is same and no major difference for temperature in PCM because the fins are not close to the point in other models without fins. Figure 18 shows the temperature distribution at top side of the model at time 20 000 s. Compared with the case without fins, the temperature at back is slightly higher due to the fins and the interface of melting goes deeper. The use of fins provides improved thermal control.

Figure 19 shows velocity distribution in air duct at time 20 000 s, compared with Figure 15, an average 5% of increase in velocity is achieved when applying fins inside. Figure 20 shows

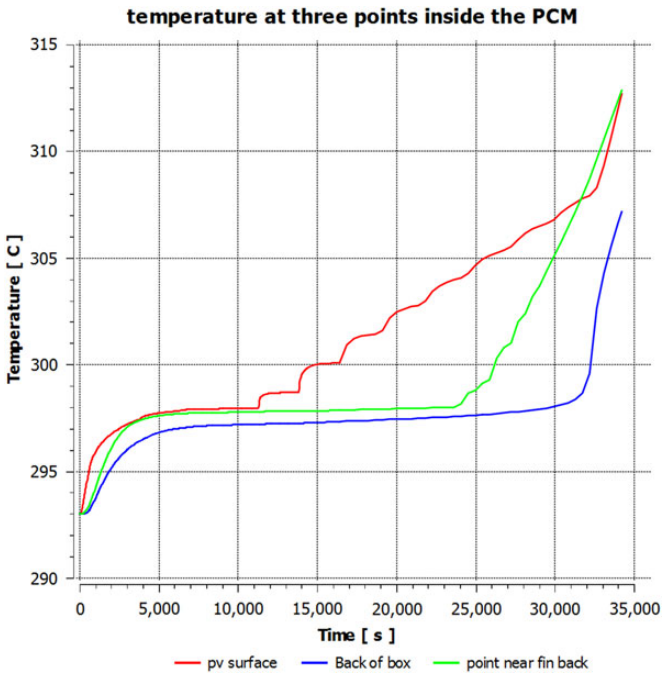

Figure 17. *Temperature at three observed points in PCM.*

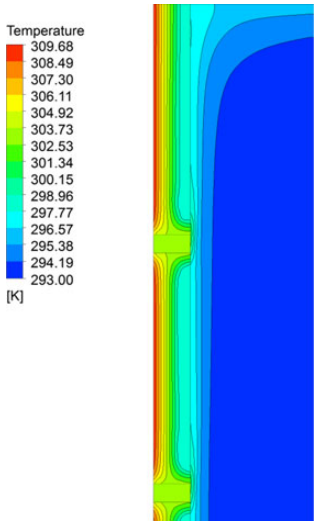

Figure 18. *Temperature distribution at top side of model at time 20 000 s.*

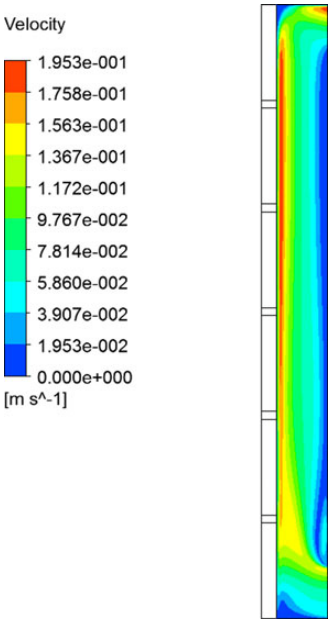

Figure 19. *Velocity distribution in air duct at 20 000 s.*

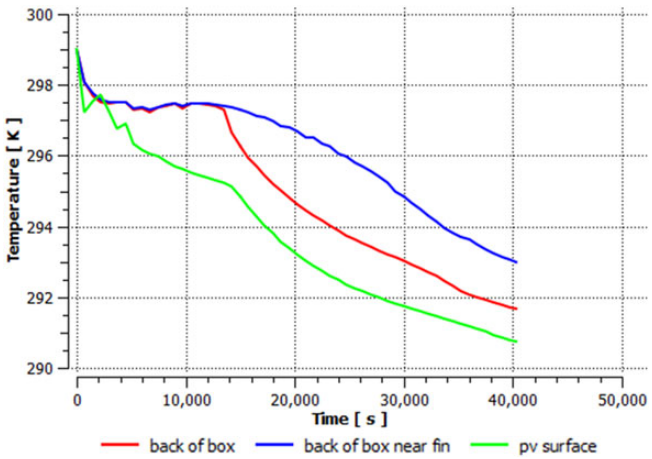

Figure 20. *Temperature variation in PCM in solidifying process.*

the temperature variation in PCM in solidifying process. It takes much short time for solidifying which may be helpful in hot night condition.

4 CONCLUSIONS

The objective of this study was to improve the PV efficiency by incorporating PCM while utilizing the convective heat from PCM for controlling indoor condition. This paper presents an experimental and numerical evaluation of PCMs for thermal management of PV devices. The experiment set up was used to measure the temperature and velocity in order to validate the CFD model. The result shows that the thicker layer of PCM can provide more heat capacity for maintaining temperature, but it has lower ability for natural ventilation and presents a problem of too long time of melting and solidifying. The simulation model is applied to a typical sunny day in Nottingham which shows the system can maintain the PV temperature below its normal operating cell temperature for ~9.7 h. However, it takes almost 16.67 h for full solidification. Either forced convection or fins in the PCM are recommended to increase the heat removal. PCM with internal fins provide improved thermal control and it reduces a lot of time for solidification and increases natural ventilation. The test rig and the simulation model will be extended to evaluate the

performance of typical houses integrated with the PV/PCM system for different weather conditions in the future.

REFERENCES

[1] Biwole PH, Eclache P, Kuznik F. Phase-change materials to improve solar panel's performance. *Energy Buildings* 2013;**62**:59–67.

[2] Hasan A, McCormack SJ, Huang MJ, *et al*. Energy and cost saving of a photovoltaic-phase change materials (PV-PCM) system through temperature regulation and performance enhancement of photovoltaics. *Energies* 2014;**7**:1318–31.

[3] Chandrasekara M, Sureshb S, Senthilkumara T, *et al*. Passive cooling of standalone flat PV module with cotton wick structures. *Energ Convers Manage* 2013;**71**:43–50.

[4] Meia L, Infieldb D, Eickerc U, *et al*. Cooling potential of ventilated PV façade and solar air heaters combined with a desiccant cooling machine. *Renew Energy* 2006;**31**:1265–78.

[5] Yun GY, McEvoy M, Steemers K. Design and overall energy performance of a ventilated photovoltaic façade. *Solar Energy* 2007;**81**:383–94.

[6] Sari A, Karaipekli A. Thermal conductivity and latent heat thermal energy storage characteristics of paraffin/expanded graphite composite as phase change material. *Appl Therm Eng* 2007;**27**:1271–7.

[7] Zalba B, Marin JM, Cabeza LF, *et al*. Review on thermal energy storage with phase change: materials, heat transfer analysis and applications. *Appl Therm Eng* 2003;**23**:251–83.

[8] Ismail KAR, Alves CLF, Modesto MS. Numerical and experimental study on the solidification of PCM around a vertical axially finned isothermal cylinder. *Appl Therm Eng* 2001;**21**:53–77.

[9] Huang MJ, Eames PC, Norton B. Phase change materials for limiting temperature rise in building integrated photovoltaics. *Solar Energy* 2006;**80**:1121–30.

[10] Huang MJ, Eames PC, Norton B, *et al*. Natural convection in an internally finned phase change material heat sink for the thermal management of photovoltaics. *Solar Energy Materials Solar Cells* 2011;**95**:1598–603.

[11] Huang MJ, Eames PC, Norton B. Comparison of a small-scale 3D PCM thermal control model with a validated 2D PCM thermal control model. *Sol Energy Mater Sol Cells* 2006;**90**:1961–72.

[12] Shatikian V, Ziskan G, Letan R. Numerical investigation of a PCM-based heat sink with internal fins. *International Journal of Heat and Mass Transfer* 2005;**48**:3689–3706.

[13] ANSYS Fluent 6.3 User Guide; Release 13.0, November 2010.

[14] Susman G, Dehouche Z, Cheechern T, *et al*. Tests of prototype PCM 'sails' for office cooling. *Appl Therm Eng* 2011;**31**:717–26.

[15] Assis E, Ziskind G, Letan R. Numerical and experimental study of solidification in a spherical shell. *J Heat Transfer* 2009;**131**:024502.